CANCER

Recruitment of CD103$^+$ dendritic cells via tumor-targeted chemokine delivery enhances efficacy of checkpoint inhibitor immunotherapy

John-Michael Williford[1]*, Jun Ishihara[1]*, Ako Ishihara[1], Aslan Mansurov[1], Peyman Hosseinchi[1], Tiffany M. Marchell[1,2], Lambert Potin[1,3], Melody A. Swartz[1,2,4], Jeffrey A. Hubbell[1,2†]

Although a clinical breakthrough for cancer treatment, it remains that a minority of patients respond to checkpoint inhibitor (CPI) immunotherapy. The composition of tumor-infiltrating immune cells has been identified as a key factor influencing CPI therapy success. Thus, enhancing tumor immune cell infiltration is a critical challenge. A lack of the chemokine CCL4 within the tumor microenvironment leads to the absence of CD103$^+$ dendritic cells (DCs), a crucial cell population influencing CPI responsiveness. Here, we use a tumor stroma–targeting approach to deliver CCL4; by generating a fusion protein of CCL4 and the collagen-binding domain (CBD) of von Willebrand factor, we show that CBD fusion enhances CCL4 tumor localization. Intravenous CBD-CCL4 administration recruits CD103$^+$ DCs and CD8$^+$ T cells and improves the antitumor effect of CPI immunotherapy in multiple tumor models, including poor responders to CPI. Thus, CBD-CCL4 holds clinical translational potential by enhancing efficacy of CPI immunotherapy.

INTRODUCTION

Cancer immunotherapy has been a breakthrough treatment strategy for a number of malignancies, activating the immune system to identify and kill cancer cells (*1*). In particular, checkpoint inhibitor (CPI) antibodies, which block key inhibitory pathways involved in T cell activation, have shown significant clinical potential in a number of solid tumors, leading to extended patient survival (*2*). While these therapies trigger antitumor immunity in a minority of patients, a significant fraction do not respond to CPI therapies (*3*). For example, a recent trial combining nivolumab (anti–programmed cell death protein 1, anti–PD-1) and ipilimumab (anti-cytotoxic T-lymphocyte–associated protein 4, anti–CTLA-4) induced only 11.5% complete response and 57.6% objective response in patients with melanoma (*4*).

To better understand why certain tumors do not respond to CPI therapy, a number of studies have aimed to investigate the phenotype of the tumor microenvironment (*5*). One key aspect influencing response to CPI therapy involves the magnitude and composition of immune cell infiltration into the tumor (*6*, *7*). From this, tumors can be broadly categorized as being inflamed or noninflamed, often referred to as exhibiting a hot or cold phenotype (*8*). Inflamed, or hot, tumors are infiltrated by a large number of CD8$^+$ cytotoxic T cells and antigen-presenting cells such as dendritic cells (DCs) (*9*); these tumors correlate with the greatest tumor regression when treated with CPI antibody therapies (*10*). On the other hand, noninflamed, or immunologically cold, tumors are characterized by a low number of CD8$^+$ T cells, instead being populated by suppressor cells such as regulatory T cells (T_{regs}) or myeloid-derived suppressor cells (MDSCs) (*11*). Noninflamed tumors are further stratified as immune-excluded or immune-desert phenotypes (*12*). Immune-excluded tumors may have T cell infiltration, although it is usually localized to the periphery. On the other hand, immune-desert phenotypes exhibit a lack of infiltrating T cells into the tumor. Noninflamed tumors correlate with poor responses to CPI therapy (*13*).

Enhancing T cell infiltration into tumors, therefore, is a promising strategy to improve the fraction of patients that respond to cancer immunotherapy (*14*). Detailed mechanistic studies of the tumor microenvironment have highlighted a crucial subset of DCs, CD103$^+$ migratory DCs, as key drivers of antitumor immunity (*15*–*17*). While they comprise less than 5% of the myeloid cells in the tumor, CD103$^+$ DCs are highly effective at trafficking intact antigen to the draining lymph nodes (*16*), where it can be cross-presented to CD8$^+$ T cells to prime antitumor immune responses (*18*). Furthermore, CD103$^+$ DCs are the main source of T cell–recruiting chemokines, namely, CXCL9 and CXCL10, in the tumor microenvironment (*19*). An absence of CD103$^+$ DCs from the tumor may therefore contribute to the noninflamed phenotype observed in some tumors.

Recent work from Spranger *et al.* (*13*, *20*) has identified a molecular signature of some melanomas that limits the recruitment of CD103$^+$ DCs into the tumor. These CPI unresponsive, noninflamed tumors lacked expression of the chemokine CCL4, which recruits CD103$^+$ DCs to the tumor through its receptor CCR5 (*20*). These results highlight the crucial role of CCL4 in the recruitment of CD103$^+$ DCs, an integral part of antitumor immune responses and subsequent effectiveness of CPI immunotherapy.

To this point, there have been no reports using CCL4 as a molecular therapy to enhance tumor immune infiltrates and subsequent effectiveness of cancer immunotherapy. To realize the therapeutic potential of CCL4, delivery and retention within the tumor are paramount to effectively recruit CD103$^+$ DCs. Broadly, targeted delivery of therapeutics is a key challenge to maximize the potential of immunotherapy (*21*). Previously, we have identified an effective strategy to target proteins to and retain them within the tumor microenvironment following systemic administration by using exposed collagen (*22*), which is accessible in tumors due to blood vessel abnormalities and hyperpermeability (*23*). This leakiness

[1]Pritzker School of Molecular Engineering, University of Chicago, Chicago, IL 60637, USA. [2]Committee on Immunology, University of Chicago, Chicago, IL 60637, USA. [3]Institute of Bioengineering, Ecole Polytechnique Fédérale de Lausanne, CH-1015 Lausanne, Switzerland. [4]Ben May Department for Cancer Research, University of Chicago, Chicago, IL 60637, USA.
*These authors contributed equally to this work.
†Corresponding author. Email: jhubbell@uchicago.edu

allows for collagen to be exposed to molecules in the bloodstream; because collagen is abundant in the tumor extracellular matrix, it presents an attractive target for tumor delivery and retention (*24*, *25*). We have shown that, either through molecular conjugation or recombinant fusion with the specific collagen-binding domain (CBD) of von Willebrand factor (VWF, specifically the A3 domain) (*26*), the therapeutic effects of CPI antibodies or the cytokine interleukin-2 (IL-2) were enhanced while minimizing off-target toxicity associated with these therapies (*22*).

Here, we hypothesize that targeted delivery of CCL4 to the tumor can enhance recruitment of $CD103^+$DCs and, subsequently, tumor immune infiltration; furthermore, when combined with CPI antibody therapy, this inflamed phenotype will enhance its efficacy and improve antitumor immune responses, thus holding the potential to increase the fraction of patients that respond to CPI therapy.

RESULTS

CBD-CCL4 binds to collagen and enhances accumulation within the tumor

CBD-CCL4 recombinant protein was produced using mammalian protein expression techniques similar to our previous report (*22*). Following production and purification using affinity and size-exclusion chromatography, CBD-CCL4 was evaluated using SDS–polyacrylamide gel electrophoresis (SDS-PAGE). Fusion with CBD increased the molecular size of CCL4 by approximately 20 kDa compared to native CCL4, consistent with the size of the A3 domain of VWF (Fig. 1A). Using dynamic light scattering to measure protein size, we have confirmed that CBD-CCL4 does not form high–molecular weight aggregates during routine storage and handling, as well as in mouse serum (fig. S1). Using surface plasmon resonance (SPR), we calculated the dissociation constant (K_D) for binding to collagen I and collagen III as 33.4 and 14.5 nM, respectively (Fig. 1, B and C). These results agree with previous collagen affinity measurements for CBD-modified immunotherapies (*22*). Native [wild-type (WT)] CCL4 did not show any detectable affinity for either collagen I or collagen III from both mouse and human origin (fig. S2A). Furthermore, CBD-CCL4, but not WT CCL4, colocalized with collagen I in human melanoma tumor cryosections (Fig. 1, D and E), showing the strongest signal around the blood vasculature where collagen I was densest. Similar staining patterns were observed for murine melanoma cryosections (fig. S2B). These observations confirm that CBD-CCL4 can bind to collagen encountered in the tumor microenvironment. Next, we evaluated the activity of WT CCL4 and CBD-CCL4 using a calcium flux assay, as CCL4 signals through the G protein–coupled receptor (GPCR) CCR5 (*27*), leading to intracellular calcium elevation upon activation (Fig. 1F). Both WT CCL4 and CBD-CCL4 exhibited similar GPCR activation levels, highlighting that CBD fusion did not alter the ability of CCL4 to signal through CCR5.

Moving to an in vivo system, we evaluated the blood plasma pharmacokinetics of WT CCL4 and CBD-CCL4 following intravenous administration in B16F10 tumor-bearing mice. CBD-CCL4 exhibited modestly delayed clearance compared to WT CCL4 (Fig. 1G). To confirm that CBD fusion enhanced tumor delivery of CCL4, we performed biodistribution studies in established (>100 mm^3) orthotopic EMT6 breast cancer–bearing mice following intravenous administration. CBD-CCL4 fusion exhibited a 2.4-fold increase in tumor accumulation 30 min following administration, when both WT CCL4 and CBD-CCL4 are cleared from plasma (Fig. 1H and fig. S3). These data demonstrate the effective accumulation of CBD-CCL4 within the tumor microenvironment.

CBD-CCL4 enhances efficacy of CPI therapy in B16F10 melanomas and EMT6 breast tumors through recruitment of DCs and T cells and synergizes with anti–PD-1 CPI therapy

We next investigated whether treatment with CBD-CCL4 could enhance tumor immune infiltration, a key factor driving successful responses to CPI therapy. For all subsequent experiments, CCL4 chemokine therapy was coadministered with CPI therapy comprising αCTLA4 and anti-programmed death-ligand 1 (αPD-L1), a combination treatment used for advanced melanoma and non–small cell lung cancer in the clinic (*28*, *29*). CPI therapy alone was included for baseline comparison. We first evaluated combination CCL4 and CPI therapy in B16F10 melanoma, a tumor model that responds poorly to CPI therapy alone (*22*, *30*, *31*). As shown in Fig. 2A, only the combination of CBD-CCL4 (administered intravenously) and CPI therapy (administered intraperitoneally) showed a significant reduction in tumor growth rate. WT CCL4, given in combination with CPI therapy, did not show any reduction in tumor growth rates. These results confirm that targeted chemokine delivery is required to elicit a therapeutic benefit from CCL4.

Because we observed a significant slowing of tumor growth, we hypothesized that an increase in $CD103^+$ DC recruitment to the tumor may be contributing to the antitumor immune response. Six days following administration of the treatment regime, mice were euthanized, and tumors were harvested and processed for flow cytometry analysis of the immune cell infiltrates in the tumor (gating strategy shown in fig. S4). Compared to CPI therapy alone and CPI given in combination with WT CCL4, CPI therapy given with CBD-CCL4 significantly increased the number of $CD45^+$ immune cells (Fig. 2B) in the tumor, indicating a more inflamed microenvironment. Looking specifically at the immune cell composition, we observed that CPI therapy given with CBD-CCL4 led to the highest infiltration of key drivers of antitumor immune responses, including $CD103^+$ DCs (Fig. 2C), total $CD11c^+$ DCs (Fig. 2D), $CD8^+$ T cells, both total and $CD44^+$ effector cells (Fig. 2E and fig. S5A), and natural killer (NK) cells (Fig. 2F). $CD4^+$ T cells were also significantly elevated relative to the combination of CPI therapy and WT CCL4 (Fig. 2G). No increase in the T_{reg} fraction of $CD4^+$ T cells was observed (Fig. 2H), indicating that increases in tumor inflammation did not also significantly alter the immune suppressive T_{reg} recruitment. CBD-CCL4 also did not exhibit an increase in MDSCs relative to CPI therapy alone (fig. S5B). While we observed an increase in $CD11b^+$ $F4/80^+$ macrophages in the tumor (fig. S5, C and D), they exhibited an $MHCII^{HI}$ phenotype, as opposed to an $MHCII^{Lo}$ phenotype associated with tumor progression (*32*).

Encouraged by these results, we performed correlation analysis between immune cell infiltration and tumor growth to highlight the contribution of each cell population in driving antitumor immunity. Negative correlation between tumor volume and cell infiltration was strongest for $CD103^+$ DCs ($P < 0.0001$) and $CD8^+$ T cells ($P < 0.0001$) (Fig. 2, I and J), with the greatest cell infiltrate numbers leading to the smallest tumor volumes. As expected, a significant positive correlation between $CD103^+$ DCs and $CD8^+$ T cells ($P < 0.0001$) was observed (Fig. 2K), as it has previously been shown that $CD103^+$ DCs secrete chemokines necessary for T cell infiltration into the tumor (*19*). Lesser trends were observed between NK cells ($P = 0.003$) and $CD11c^+$ DCs ($P = 0.09$) (Fig. 2, L and M), highlighting that these cell types are

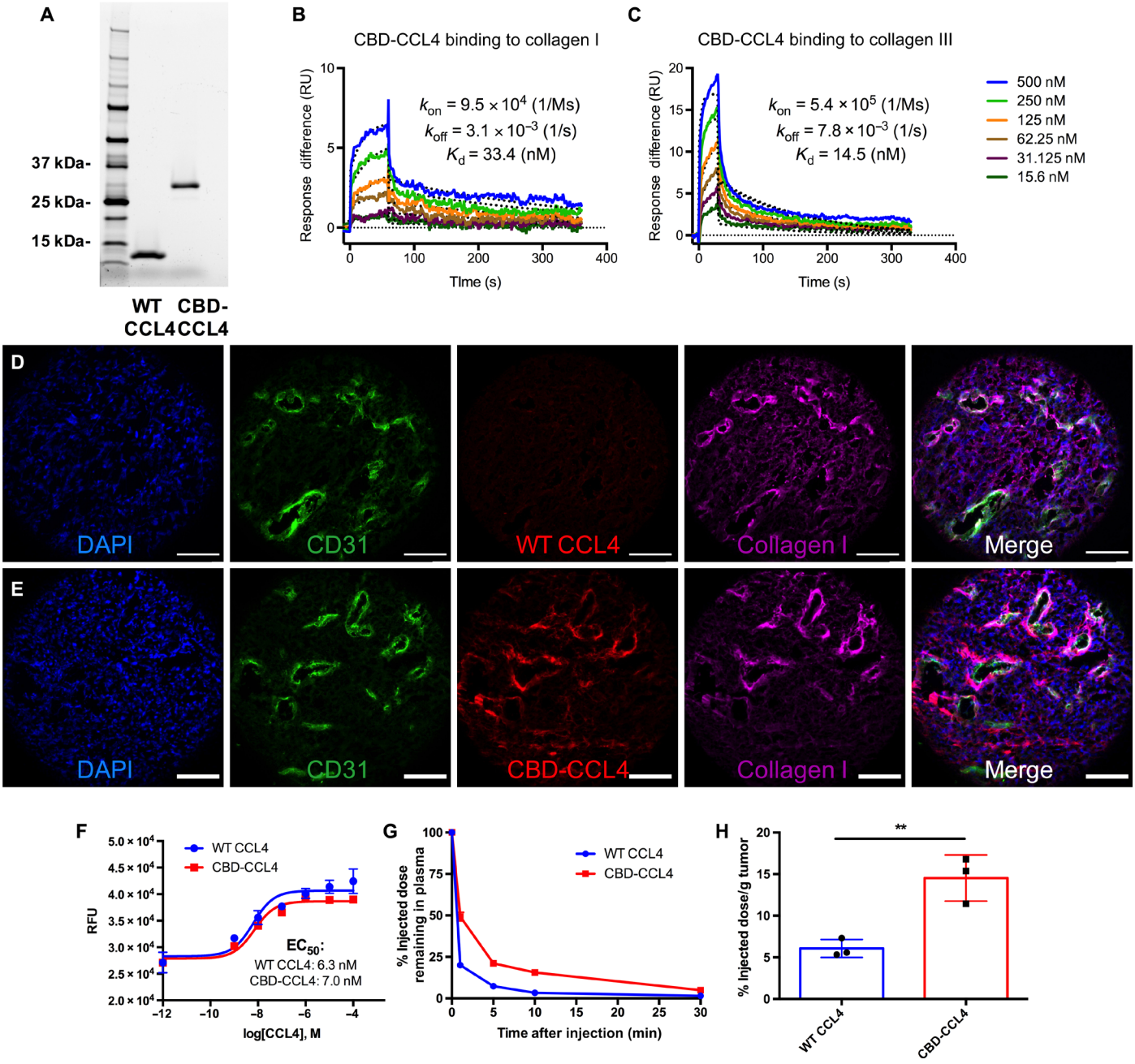

Fig. 1. CBD-CCL4 exhibits high affinity to collagen and accumulates in tumor following intravenous injection. (**A**) WT CCL4 and CBD-CCL4 were analyzed by SDS-PAGE followed by Coomassie blue staining. (**B** and **C**) Affinity of CBD-CCL4 against (B) collagen I and (C) collagen III was measured by SPR. SPR chips were functionalized with collagen I [~500 resonance units (RU)] and collagen III (~700 RU), and CBD-CCL4 was flowed over the chips at indicated concentrations. Curves represent the obtained specific responses (in resonance units) to CBD-CCL4. Experimental curves were fitted with 1:1 Langmuir fit model. Binding kinetics values [dissociation constants (K_d) and rate constants (k_{on} and k_{off})] determined from the fitted curves are shown. (**D** and **E**) Binding of (D) WT CCL4 or (E) CBD-CCL4 to human melanoma cryosections as determined by immunofluorescence microscopy. Scale bars, 100 μM. DAPI, 4′,6-diamidino-2-phenylindole. (**F**) GPCR activation assay comparing signaling of WT CCL4 and CBD-CCL4 in THP1 monocytes. Median effective concentration (EC_{50}) values were calculated using a nonlinear dose-response curve fit model. Each point represents mean ± SEM, $n = 3$. (**G**) Blood plasma pharmacokinetics was analyzed using DyLight 800–labeled WT CCL4 or CBD-CCL4 in B16F10 melanoma. Four days after tumor inoculation, mice were administered 25 μg of WT CCL4 or the molar equivalent of CBD-CCL4 (25 μg of CCL4 basis or 93 μg of CBD-CCL4) via intravenous injection. Blood was collected at the indicated time points, and plasma was separated and analyzed for CCL4 concentration. Each point represents mean ± SEM, $n = 4$. (**H**) Biodistribution was analyzed using DyLight 647–labeled WT CCL4 or CBD-CCL4 in EMT6 breast cancer. When the tumor volume reached 500 mm^3, 25 μg of WT CCL4 or the molar equivalent of CBD-CCL4 (25 μg of CCL4 basis or 93 μg of CBD-CCL4) was given via intravenous injection. Fluorescence intensity in each tumor was measured using an in vivo imaging system (IVIS), converted to percent injected dose using a known standard series, and normalized to the weight of the tumor. Each bar represents mean ± SEM, $n = 3$. **$P < 0.01$.

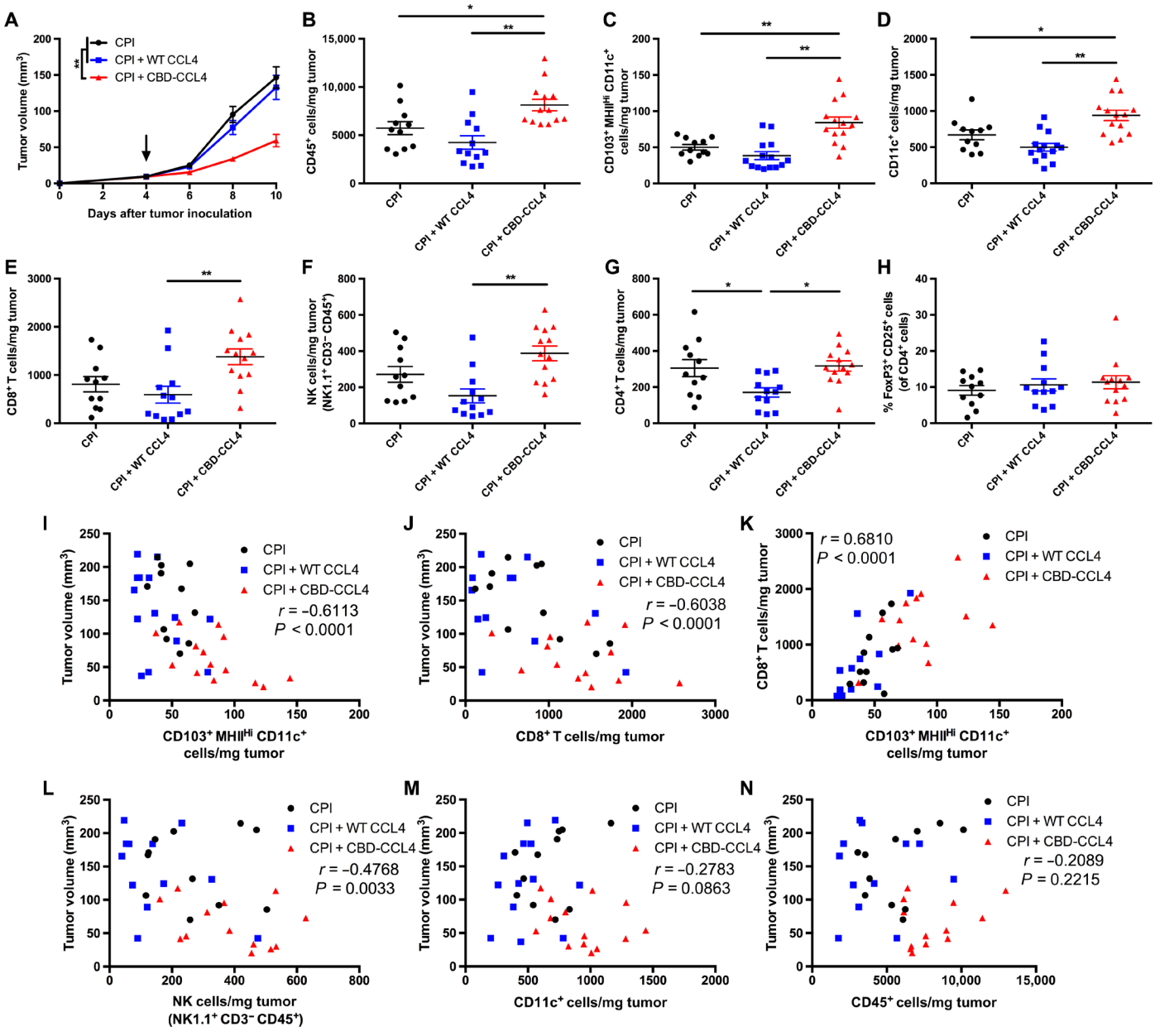

Fig. 2. CBD-CCL4 fusion recruits DCs and T cells and improves efficacy of CPI therapy in B16F10 melanoma. Mice were intradermally injected with 5×10^5 cells; 4 days later, mice were treated with WT CCL4 (25 μg given via intravenous injection) or molar equivalent CBD-CCL4 (25 μg of CCL4 basis or 93 μg of CBD-CCL4, given via intravenous injection) in combination with CPI antibody therapy consisting of αPD-L1 and αCTLA4 (100 μg each) given via intraperitoneal injection. CPI therapy alone was administered as control. (**A**) Tumor growth was monitored over time until 10 days after tumor inoculation, at which point tumors were harvested and processed for flow cytometry analysis. (**B** to **H**) Immune cell composition was evaluated, where graphs depict the number of (B) $CD45^+$ leukocytes, (C) $CD103^+$ $CD11c^+$ $MHCII^{Hi}$ DCs, (D) total $CD11c^+$ DCs, (E) $CD8^+$ T cells, (F) $NK1.1^+$ $CD3^-$ NK cells, (G) $CD4^+$ T cells, and (H) % $FoxP3^+$ $CD25^+$ T_{regs} (of total $CD4^+$ T cells). Bars represent means ± SEM, $n = 11$ to 13. $^*P < 0.05$ and $^{**}P < 0.01$. Arrow in (A) indicates time of treatment. (**I** to **N**) Regression analysis comparing the number of tumor-infiltrating cells with tumor volume was performed using the results obtained in (A) to (H). Correlations between (I) tumor volume and $CD103^+$ $CD11c^+$ $MHCII^{Hi}$ DCs, (J) tumor volume and $CD8^+$ T cells, (K) $CD103^+$ $CD11c^+$ $MHCII^{Hi}$ DCs and $CD8^+$ T cells, (L) tumor volume and $NK1.1^+$ $CD3^-$ NK cells, (M) tumor volume and total $CD11c^+$ DCs, and (N) tumor volume and total $CD45^+$ leukocytes.

important for tumor growth control, albeit less so than $CD103^+$ DCs and $CD8^+$ T cells. Furthermore, no significant correlation was observed between total $CD45^+$ immune cells and tumor growth ($P = 0.22$) (Fig. 2N), indicating that total immune infiltration alone is not strong enough to drive antitumor immunity. Rather, the specific cell types driving antitumor immunity must be recruited to maximize therapeutic effect. Last, no significant correlation was observed between tumor volume and MDSCs ($P = 0.4$) or macrophages ($P = 0.26$) (fig. S5, E and F).

To follow up on the immune infiltrate responses observed in B16F10 melanoma, we performed similar analysis in the EMT6 breast cancer model. The EMT6 model, which moderately responds to CPI therapy, is categorized as an immune-excluded tumor model (*22*, *33*).

Therefore, we hypothesized that tumor-targeted CCL4 delivery may further enhance CD103$^+$ DC recruitment and further improve efficacy of CPI therapy. Similar to the results observed in B16F10 melanoma, only the combination of CPI therapy and CBD-CCL4 exhibited a significant reduction in tumor growth (Fig. 3A). WT CCL4 given in combination with CPI therapy showed no significant improvement relative to CPI therapy alone. Detailed analysis of the immune cell infiltrates using flow cytometry found that CBD-CCL4 in combination with CPI therapy exhibited a significant increase in the total number of CD45$^+$ immune cells (Fig. 3B). Specifically, CBD-CCL4 combination therapy mediated the highest recruitment of CD103$^+$ DCs, CD8α^+ cross-presenting DCs, and total CD11c$^+$ DCs (Fig. 3, C to E). A significant increase in CD8$^+$ T cells was also observed (Fig. 3F). CBD-CCL4 combination therapy did not increase recruitment of CD4$^+$ T cells, nor did it enhance the fraction of T_{regs} in the CD4$^+$ T cell compartment (Fig. 3, G and H). Furthermore, we performed immunohistochemical analysis of the tumors, which correlated with the results from the flow cytometry study (fig. S6). Only mice treated with CPI in combination with CBD-CCL4 exhibited significant infiltration of CD8$^+$ cells.

Extending from these results, we next investigated whether CBD-CCL4 could synergize with anti–PD-1 antibody (αPD-1, CD279), another clinically approved immunotherapy for a number of indications, including melanoma, non–small cell lung cancer, bladder cancer, renal cell carcinoma, and hepatocellular carcinoma (*29*). Using two syngeneic colon cancer models, CT26 and MC38, we found that the combination of αPD-1 therapy and CBD-CCL4 mediated the slowest tumor growth rates in both models, significantly enhancing therapeutic benefit relative to αPD-1 therapy alone or combination with WT CCL4 (fig. S7, A and B). These results highlight that CBD-CCL4 can be combined with multiple CPI antibody therapies to improve therapeutic effect. Together, these results once again highlight the importance of targeted CCL4 delivery in the recruitment of key cell populations to enhance the efficacy of CPI therapy.

CBD-CCL4 therapy does not exhibit off-target immune-related adverse effects

Our previous results indicated that CBD-targeted immunotherapies exhibited a reduction in off-target treatment-related adverse events (*22*). We similarly evaluated off-target side effects following CCL4 therapy. Alanine aminotransferase (ALT), a common serum marker of liver damage, showed no differences among treatment groups (Fig. 4A). Similarly, no differences in serum levels of interferon-γ (IFN-γ) or IL-6, two common proinflammatory cytokines associated with systemic immune cell activation, were observed (Fig. 4, B and C). Last, histological analysis was performed on tissue sections taken from the lung, kidney, and liver following treatment. In all cases, no morphological damage was observed (Fig. 4D); no differences in leukocyte infiltration were seen following treatment, indicating that CBD-CCL4 therapy did not noticeably recruit immune cells to other organs under tested conditions. These results highlight that CBD-CCL4 therapy was well tolerated following systemic administration.

CPI and CBD-CCL4 combination therapy requires Batf3-lineage DCs and mediates antitumor immune response through downstream recruitment of effector T cells

We next investigated whether Batf3-lineage DCs, including CD103$^+$ DCs, were required for antitumor efficacy. We treated B16F10

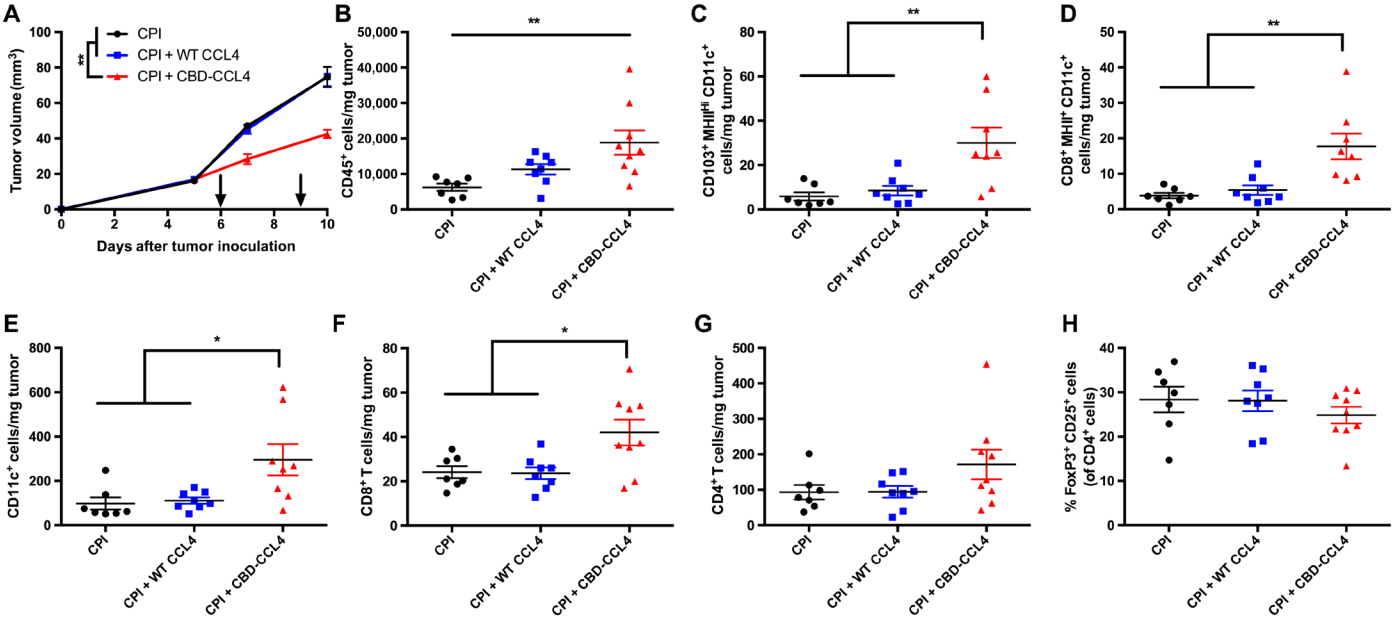

Fig. 3. CBD-CCL4 combination treatment recruits cross-presenting DCs and T cells and improves efficacy of CPI therapy in EMT6 immune-excluded breast cancer. Mice were subcutaneously injected with 5×10^5 cells; 6 and 9 days after inoculation, the mice were treated with WT CCL4 (25 μg given via intravenous injection) or molar equivalent CBD-CCL4 (25 μg of CCL4 basis or 93 μg of CBD-CCL4, given via intravenous injection) in combination with CPI antibody therapy consisting of αPD-L1 and αCTLA4 (100 μg each) given via intraperitoneal injection. CPI therapy alone was administered as control. (**A**) Tumor growth was monitored over time until 10 days after tumor inoculation, at which point tumors were harvested and processed for flow cytometry analysis. (**B** to **H**) Immune cell composition was evaluated, where graphs depict the number of (B) CD45$^+$ leukocytes, (C) CD103$^+$ CD11c$^+$ MHCII^{Hi} DCs, (D) CD8α^+ CD11c$^+$ MHCII^{Hi} DCs, (E) total CD11c$^+$ DCs, (F) CD8$^+$ T cells, (G) CD4$^+$ T cells, and (H) % FoxP3$^+$ CD25$^+$ T_{regs} (of total CD4$^+$ T cells). Bars represent means ± SEM, $n = 7$ to 9. *$P < 0.05$ and **$P < 0.01$ Arrows indicate time of treatment.

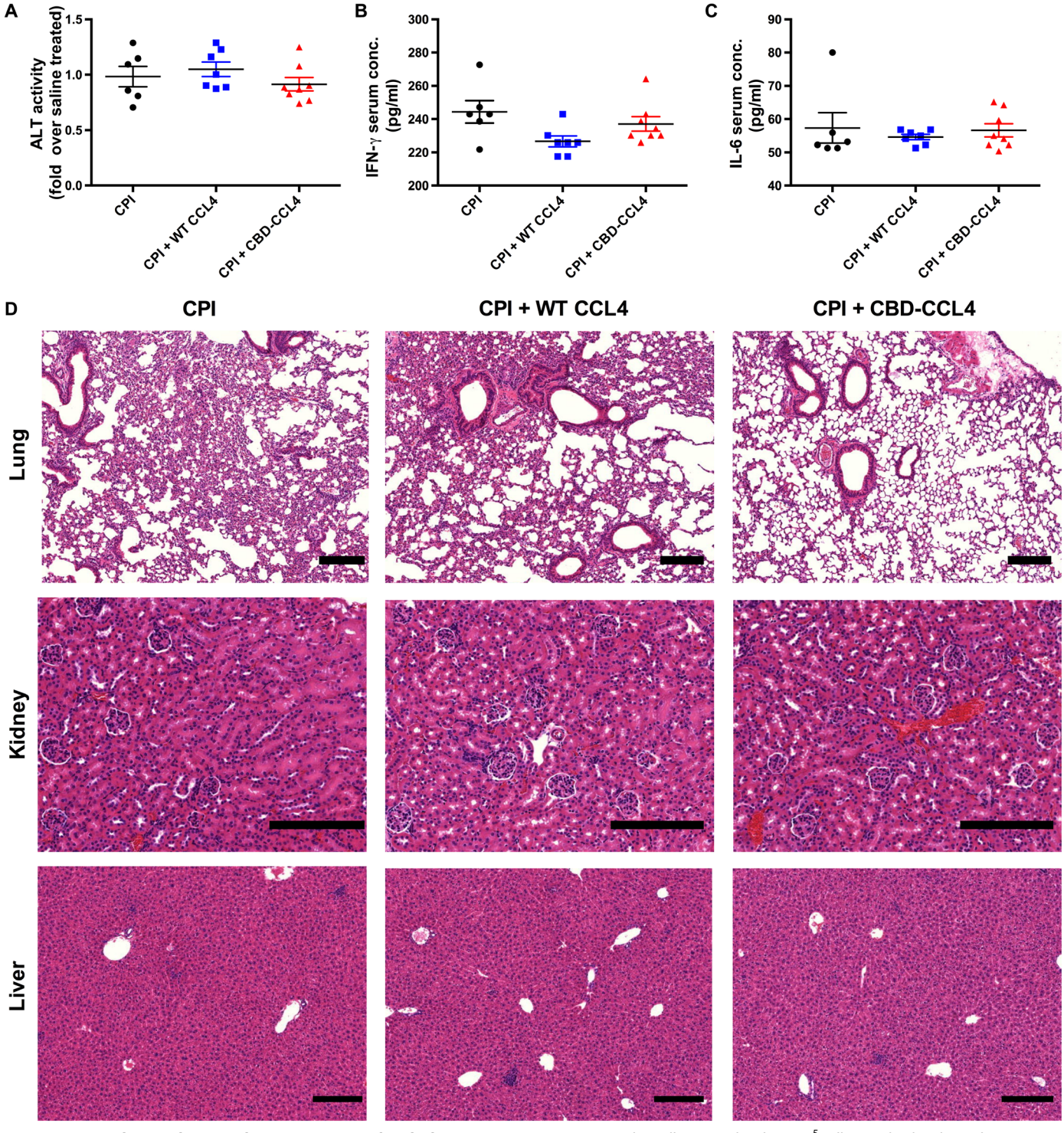

Fig. 4. CBD-CCL4 therapy does not elevate treatment-related adverse events. Mice were intradermally injected with 5×10^5 cells; 4 and 7 days later, the mice were treated with WT CCL4 (25 μg given via intravenous injection) or molar equivalent CBD-CCL4 (25 μg of CCL4 basis or 93 μg of CBD-CCL4, given via intravenous injection) in combination with CPI antibody therapy consisting of αPD-L1 and αCTLA4 (100 μg each) given via intraperitoneal injection. CPI therapy alone was administered as control. (**A**) ALT activity in serum of mice, relative to saline-treated control mice, as measured 10 days after tumor inoculation. (**B** and **C**) Eight days after tumor inoculation, blood was collected, and serum levels of (B) IFN-γ and (C) IL-6 were measured by enzyme-linked immunosorbent assay (ELISA). (**D**) Ten days after tumor inoculation, the lung, kidney, and liver were harvested, and histological analysis was performed to assess tissue morphology and immune cell infiltration. Representative images of each organ are shown. Scale bars, 200 μm. All bars represent means ± SEM, $n = 6$ to 8.

tumors implanted into Batf3$^{-/-}$ mice (*34*) with either CPI alone or CPI in combination with CBD-CCL4. No differences in treatment efficacy were observed (Fig. 5A), highlighting the importance in recruiting CD103$^+$ DCs to enhance CPI therapy. In addition, we performed detailed immune cell profiling of B16F10 tumors implanted in Batf3$^{-/-}$ mice. No significant differences were observed for CD45$^+$ cells, CD103$^+$ DCs, total CD11c$^+$ DCs, CD8$^+$ T cells, CD4$^+$ T cells, or NK cells (Fig. 5 B to G). Compared to results shown above in WT mice, the magnitude of immune cell recruitment decreased greater than 80% in Batf3$^{-/-}$ mice. Encouraged by these results, we next investigated whether CBD-CCL4 combination therapy mediated antitumor efficacy through downstream recruitment of effector T cells. As mentioned previously, CD103$^+$ DCs are the main source of CXCL9 and CXCL10 (*19*), which recruit effector T cells via CXCR3. Using B16F10 melanoma, CPI and CBD-CCL4 combination therapy slowed tumor growth and enhanced survival (Fig. 5, H and I). However, when CXCR3 signaling was blocked, CPI and CBD-CCL4 combination therapy lost its antitumor efficacy, suggesting that CBD-CCL4 mediates its therapeutic effect via CD103$^+$ DC-driven T cell recruitment. B16F10 melanoma treated with CBD-CCL4 alone showed

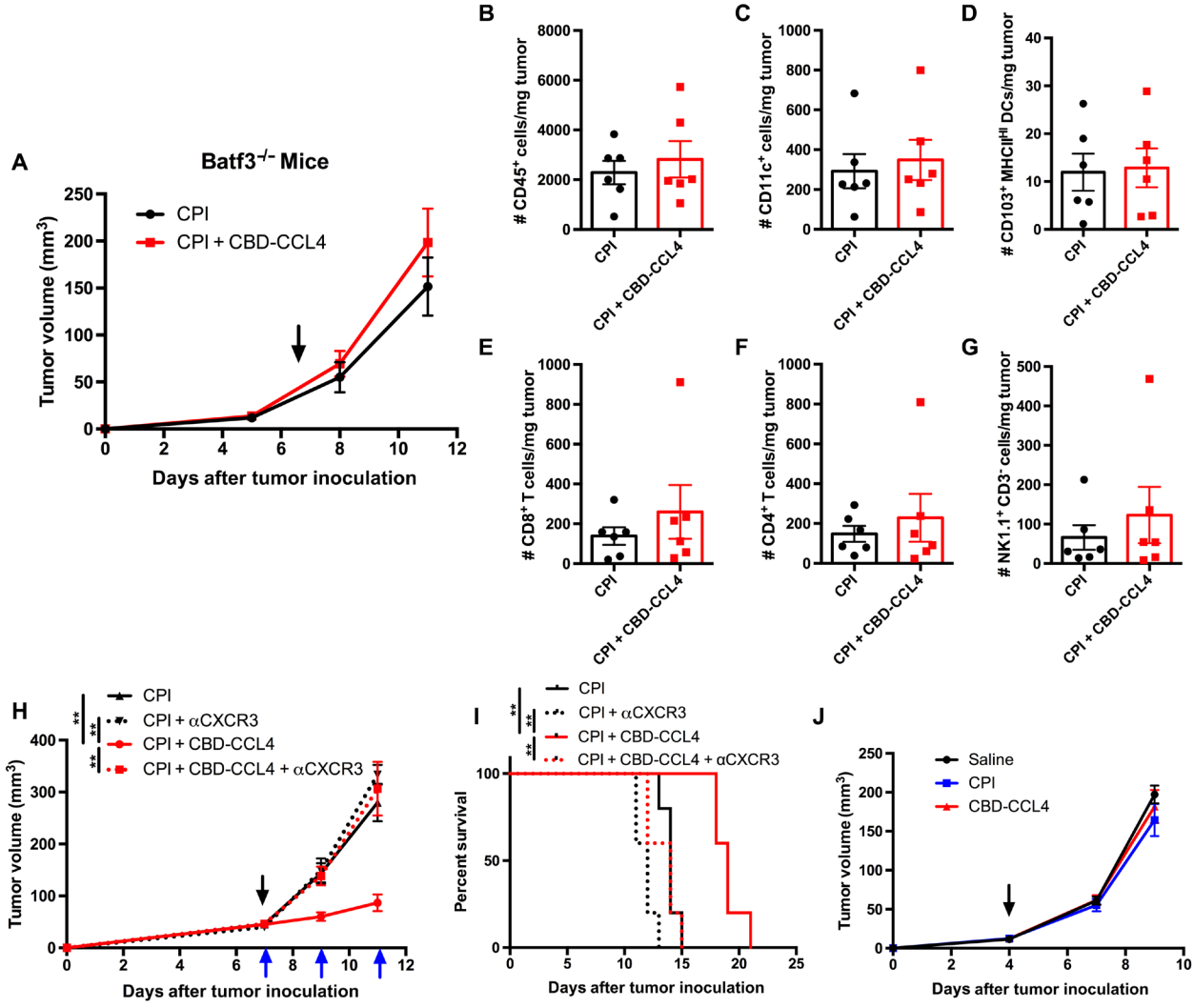

Fig. 5. CBD-CCL4 requires Batf3-lineage DCs and mediates downstream effector T cell recruitment. (**A** to **G**) Batf3$^{-/-}$ mice were intradermally injected with 5×10^5 B16F10 cells; 7 days later, once tumor volume exceeded 50 mm^3, the mice were treated with CBD-CCL4 (25 μg of CCL4 basis or 93 μg of CBD-CCL4, given via intravenous injection) in combination with CPI antibody therapy consisting of αPD-L1 and αCTLA4 (100 μg each) given via intraperitoneal injection. CPI therapy alone was administered as comparison. Graphs display (A) tumor growth curves and (B to G) tumor immune infiltrates depicting the number of (B) CD45$^+$ leukocytes, (C) total CD11c$^+$ DCs, (D) CD103$^+$ CD11c$^+$ MHCII^{Hi} DCs, (E) CD8$^+$ T cells, (F) CD4$^+$ T cells, and (G) NK cells. Graphs depict means ± SEM, $n = 6$. $^{**}P < 0.01$. (**H** and **I**) C57BL/6 mice were intradermally injected with 5×10^5 B16F10 cells; 7 days later, the mice were treated with CBD-CCL4 (25 μg of CCL4 basis or 93 μg of CBD-CCL4, given via intravenous injection) in combination with CPI antibody therapy consisting of αPD-L1 and αCTLA4 (100 μg each) given via intraperitoneal injection, as shown with a black arrow. CPI therapy alone was administered as comparison. In addition, indicated groups were treated with 200 μg of CXCR3 blocking antibody via intraperitoneal injection on days 7, 9, and 11, as shown by blue arrows. (H) Tumor growth curves and (I) survival curves are shown, with each bar representing mean ± SEM, $n = 5$. (**J**) C57BL/6 mice were intradermally injected with 5×10^5 B16F10 cells; 4 days later, the mice were treated with saline, CBD-CCL4 (25 μg of CCL4 basis or 93 μg of CBD-CCL4, given via intravenous injection) or CPI antibody therapy consisting of αPD-L1 and αCTLA4 (100 μg each) given via intraperitoneal injection. Tumor growth curves are shown, with each bar representing mean ± SEM, $n = 5$. $^{**}P < 0.01$. Arrows indicate time of treatment.

no reduction in tumor growth relative to saline control or CPI therapy alone (Fig. 5J), highlighting the importance of combination with CPI therapy in maximizing the effect of CCL4 therapy. It is unlikely that CBD-CCL4 directly recruits T cells via CCR5, as previous reports suggest that CCR5 expression is significantly higher on DCs compared to T cells (*35*). Staining for cell surface CCR5 expression confirmed these findings, as shown in fig. S8.

CPI and CBD-CCL4 codelivery enhances antitumor efficacy in orthotopic and spontaneous breast cancer models

Last, we investigated the efficacy of combination therapy in both orthotopic implantable and spontaneous breast cancer models. Following a single administration of CPI in combination with CBD-CCL4 in orthotopic implanted MMTV-PyMT tumor-bearing mice, 50% of tumors were completely cleared; conversely, only 10% of mice treated with CPI therapy alone became tumor free (Fig. 6A). Survival analysis also showed a significant improvement following combination therapy with CPI and CBD-CCL4 (Fig. 6B). Encouraged by these results, we rechallenged mice that had cleared tumors following CBD-CCL4 therapy in the contralateral mammary fat pad. Compared with naïve control mice (i.e., previously naïve mice given a tumor inoculation), which all developed tumors, no mice that had demonstrated complete response after treatment with CBD-CCL4 combination therapy developed tumors following a second tumor challenge (Fig. 6C). These results indicate that long-term immunologic memory was established. To further understand the mechanism for tumor clearance, the rechallenged mice were euthanized, and spleens were collected for flow cytometric analysis. Following stimulation with phorbol 12-myristate 13-acetate (PMA) and ionomycin, cytokine production was evaluated in splenic T cells. Both $CD8^+$ and $CD4^+$ T cells from complete-responding mice that had been treated with CPI in combination with CBD-CCL4 and rechallenged (rejecting the new tumor cells) exhibited higher percentages of cells, relative to naïve challenge controls, that were double positive for IFN-γ and tumor necrosis factor–α (TNFα), key cytokines driving antitumor immunity (Fig. 6D). Furthermore, IFN-γ production was higher in effector ($CD44^+$) T cells following CPI and CBD-CCL4 combination treatment (Fig. 6, E and F), compared to naïve control mice. These results highlight the enhanced antitumor immune response mediated by CBD-CCL4 therapy, conferring protection from secondary tumor challenges.

To this point, antitumor efficacy of CBD-CCL4 has been demonstrated in multiple implantable tumor models. While notable, these models develop rapidly, which may affect the leakiness and disordered nature of the tumor microvasculature (*36*), potentially making it more amenable to targeting via our collagen-binding approach. It is possible that slowly developing tumors, on the other hand, may not exhibit this same disordered vasculature (*37*), possibly limiting the effectiveness of CBD-CCL4 therapy. To explore this, we used female FVB/N-Tg(MMTV-PyVT)634Mul/J (MMTV-PyMT) mice, which spontaneously develop invasive ductal carcinomas in their mammary fat pads around 6 to 7 weeks after birth (*38*). This model is also histologically similar to human breast cancers (*39*), making it a suitable model to demonstrate the translational potential of CBD-CCL4 combination therapy. Once again, CBD-CCL4 in combination with CPI therapy slowed tumor growth relative to CPI therapy alone (Fig. 6G). In addition, median survival time increased to 29 days following initial treatment for the CPI and CBD-CCL4 combination therapy, compared to 23 days for CPI therapy alone (fig. S9). These results demonstrate that CBD targeting can also be applied to spontaneously developing tumors in addition to implantable tumor models.

DISCUSSION

Increasing the fraction of patients that respond to CPI therapy remains a major challenge to further boost the remarkable effects that these drugs have had for cancer treatment. Recruitment of key immune cell populations that drive antitumor immune responses, including T cells and DCs, is an attractive strategy to accomplish this goal, as these cell populations often correlate with the greatest percentage of patients that experience successful therapeutic outcomes (*15*, *16*). In this work, we used CCL4 to enhance tumor immune infiltration for two primary reasons. First, recent work from Spranger and Gajewski (*20*) has highlighted the role of CCL4 in recruiting $CD103^+$ DCs to tumors; in tumors lacking CCL4 expression, an immunologically cold phenotype was observed, and CPI therapy performed poorly. Furthermore, studies have highlighted the importance of $CD103^+$ DCs in presenting tumor-associated antigens and recruiting effector T cells to the tumor microenvironment through production of CXCL9 and CXCL10 (*19*), influencing responsiveness to CPI therapy.

To maximize the therapeutic potential of CCL4, a targeted delivery strategy must be used. Relative to WT CCL4, the increase in molecular size of the molecule may slow its clearance from blood; this could have beneficial implications for tumor targeting, as enhanced blood circulation time is often attractive for enhancing delivery of macromolecules to tumors (*40*). Furthermore, enhanced circulation time may allow for additional opportunities to bind to and be retained by exposed collagen in the leaky tumor microvasculature (*41*). The collagen-targeting delivery and retention strategy used in this work offers several distinct advantages. Collagen, as opposed to a tumor cell–specific antigen or receptor, is expressed in many different solid tumor types, which may allow this strategy to be broadly applicable without the need to stratify patients on the basis of the expression of a target protein before treatment. In addition, collagen, unlike some tumor cell surface receptors, is not subject to turnover associated with receptor endocytosis or down-regulation due to tumor cell mutations. In targeting the tumor microenvironment, our approach turns the stroma into both a target for the drug being administered and a depot for its retention and release over time. This may be of particular importance for chemokines such as CCL4, as they presumably exert their biological effect by recruiting cells through a concentration gradient. We have previously shown that our CBD-targeting approach binds to collagen within the tumor stroma following systemic administration, exploiting the disordered structure and leakiness of these vessels in solid tumors (*22*). CBD-CCL4, therefore, may localize to the tumor stroma and vasculature through collagen affinity and be slowly released over time, because of matrix remodeling or protein binding and dissociation kinetics, generating a concentration gradient through which $CD103^+$ DCs can then infiltrate the tumor and enhance responsiveness of CPI therapy.

From our results, we have confirmed in multiple tumor models that targeted delivery of CCL4 is required to observe a therapeutic effect. WT CCL4 mediated no increase in the recruitment of key drivers of antitumor immune responses, nor did it slow tumor growth when given in combination with CPI therapy. CBD-CCL4, however, given in combination with CPI therapy, significantly slowed tumor

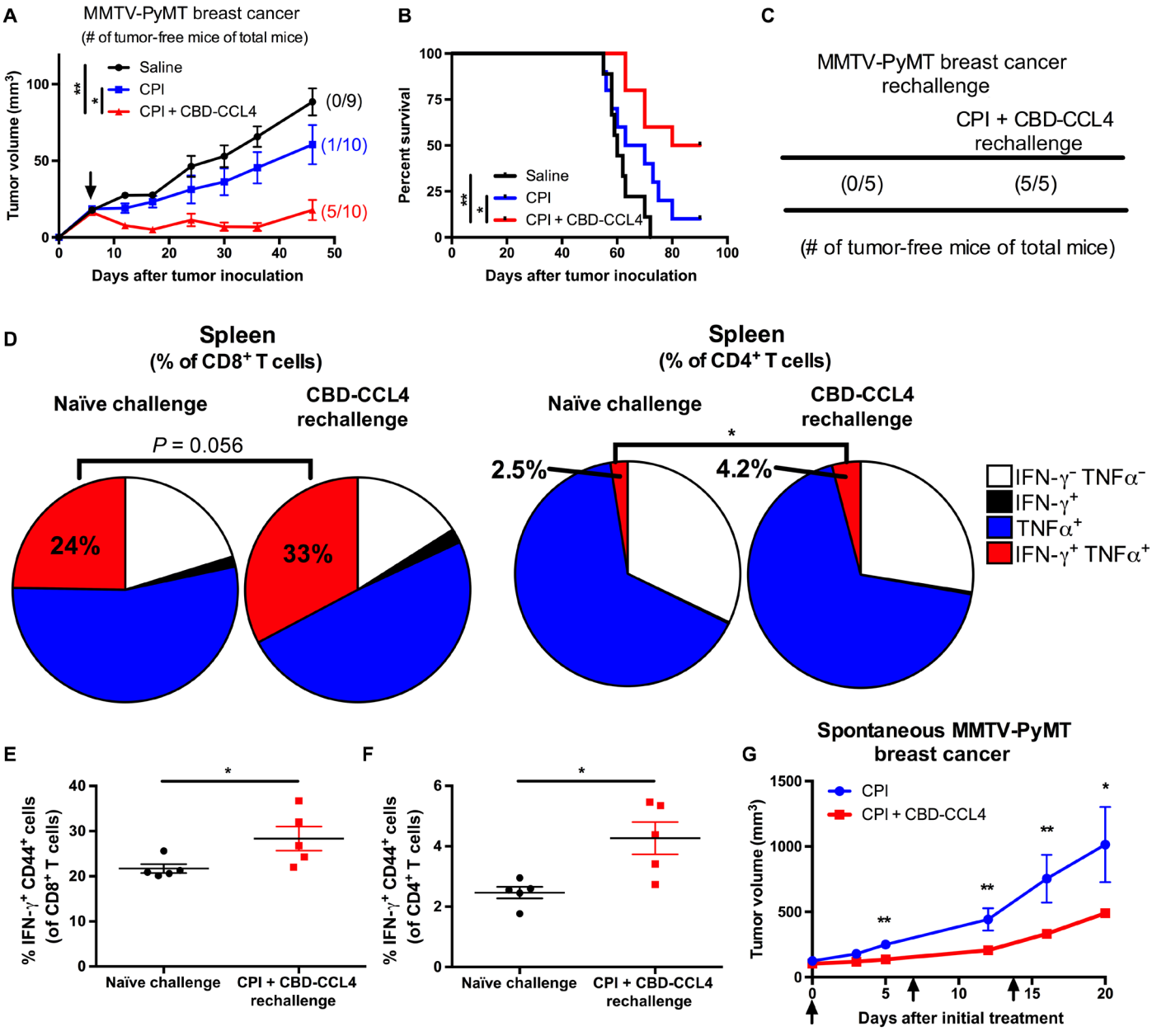

Fig. 6. CBD-CCL4 in combination with CPI slows growth of implantable and spontaneous MMTV-PyMT breast tumors. (**A** to **F**) 10^6 MMTV-PyMT cells were inoculated on the right mammary fat pad. Six days after inoculation, mice were treated with CBD-CCL4 (25 μg of CCL4 basis or 93 μg of CBD-CCL4, given via intravenous injection) in combination with CPI antibody therapy consisting of αPD-L1 and αCTLA4 (100 μg each) given via intraperitoneal injection. CPI therapy alone was administered as comparison. (A) Tumor growth curves and (B) survival curves are shown, with each bar representing mean ± SEM, $n = 9$ to 10. Numbers indicate the fraction of tumor-free mice in each group. $^*P < 0.05$ and $^{**}P < 0.01$. (C) One month after becoming tumor free, the mice were given a secondary tumor challenge with 10^6 MMTV-PyMT cells in the contralateral mammary fat pad. Naïve control mice were inoculated in a similar fashion. Numbers indicate how many mice remain tumor free 14 days following tumor challenge. (**D** to **F**) Twenty days after tumor rechallenge, the mice were euthanized, and splenocytes were stimulated with PMA and ionomycin for 6 hours to evaluate cytokine production. (D) Charts depict average percentage of splenic $CD8^+$ T cells and $CD4^+$ T cells producing the indicated cytokines. $^*P < 0.05$. (E and F) Percentage of IFN-γ–producing effector ($CD44^+$) (E) $CD8^+$ T cells and (F) $CD4^+$ T cells in the spleen. Bars represent means ± SEM, $n = 5$. $^*P < 0.05$. (**G**) Spontaneous MMTV-PyMT tumor-bearing mice were monitored until total tumor burden reached 100 mm^3. At this point, the mice were treated with CBD-CCL4 (25 μg of CCL4 basis or 93 μg of CBD-CCL4, given via intravenous injection) in combination with CPI antibody therapy consisting of αPD-L1 and αCTLA4 (100 μg each) given via intraperitoneal injection. CPI therapy alone was administered as comparison. Identical dosing was given 7 and 14 days after the initial treatment. Tumor growth curves until the first mouse died are shown. Graphs depict means ± SEM, $n = 6$. $^*P < 0.05$ and $^{**}P < 0.01$. Arrows indicate time of treatment.

growth in tumor models that respond poorly to CPI therapy alone, likely because of the recruitment of DCs and T cells. Correlation analysis supports this finding, as the most significant relationships between tumor growth and cell infiltration were found for $CD103^+$ DCs and $CD8^+$ T cells. It is important to note that recruitment of these specific cell populations is paramount for antitumor immune responses, as opposed to general $CD45^+$ immune cell infiltration, as correlations were not statistically significant when comparing tumor growth and total $CD45^+$ immune cell numbers. Although in our studies we attribute increases in efficacy to $CD103^+$ DCs, as their correlation with the smallest tumor volumes was most significant, it is possible that $CD8^+$ DCs may be contributing to this antitumor effect as well, since we observed increases in $CD8^+$ DC numbers from our EMT6 infiltrate analysis. However, $CD103^+$ DC numbers are much higher, suggesting a greater contribution to the antitumor effect.

Our initial studies do not raise any significant concerns for treatment-related off-target adverse events associated with CBD-CCL4 therapy, even in the presence of checkpoint blockade immunotherapy. Analysis of clinically relevant liver damage markers and serum cytokine levels did not show any significant increase following treatment with CBD-CCL4 in combination with CPI. This finding suggests that there may be less risk associated with future clinical development of CBD-CCL4 therapy, compared to other cytokine therapies that may have significant side effects, such as cytokine storm. Furthermore, histological analysis did not find detectable levels of leukocyte infiltration in the lungs, liver, or kidneys, suggesting that immune cell recruitment was specific to the tumor microenvironment.

Mechanistically, we have shown that $CD103^+$ DCs are required to mediate a therapeutic effect, as Batf3 knockout mice lacking this DC population did not show any benefit following CBD-CCL4 therapy in combination with CPI. Furthermore, CBD-CCL4 did not exhibit any antitumor effects as a monotherapy in B16F10 models; this finding suggests that direct recruitment of T cells via CCL4-CCR5 interaction is not a main mechanism of treatment efficacy. Rather, CBD-CCL4 serves to recruit DCs to the tumor, which, in turn, secrete CXCL9 and CXCL10 to attract effector T cells, where their antitumor effect can be activated by CPI therapy through blockade of the immune checkpoint regulatory pathways. Our study using CXCR3 blocking antibodies supports this hypothesis, as impairment of effector T cell recruitment eliminated therapeutic efficacy of CBD-CCL4 and CPI combination therapy. Highlighting the translational potential of this therapy, we have shown that CBD-CCL4 can synergize with multiple CPI antibody drugs and exhibit therapeutic effects in multiple tumor types when given via intravenous administration.

In the implantable MMTV-PyMT model, CBD-CCL4 cotreatment increased the percentage of tumor-free mice from only 10% in CPI therapy alone to 50% of the treated mice. Tumor rechallenge studies highlighted the generation of long-term immunological memory, as mice that cleared their initial challenge did not develop tumors when given a secondary tumor challenge. Mechanistic analysis found an increased presence of T cells in these mice producing crucial proinflammatory cytokines necessary for antitumor immune responses. We also observed a significant slowing of tumor growth in spontaneously developing MMTV-PyMT breast tumors treated with CBD-CCL4 in combination with CPI therapy when compared to mice given only CPI therapy. As these tumors develop slower than implantable tumors, they may better recapitulate the phenotype observed in human tumors (*39*), highlighting the translational potential of CBD-CCL4 delivery. Optimization of dosing regimens may further improve the benefit afforded by CBD-CCL4 combination therapy.

One potential drawback of CBD-based delivery strategies, including CBD-CCL4, is that it is limited to solid tumors amenable to tumor stroma targeting. In addition, as the targeting strategy uses inherent leakiness of disordered tumor vasculature, potential accumulation in other sites with exposed collagen, including wounds, may occur. While we cannot rule out accumulation in other organs from our data, our preliminary results suggest that any accumulation is not necessarily accompanied with downstream immune cell infiltration, as shown by the lack of immune cell infiltration into the lung, liver, and kidney from histological analysis. Last, while the lack of immune cell infiltration into tumors is one key factor limiting the success of CPI therapy in certain patients, other compensatory immunomodulatory mechanisms may also exist (*13*). In these cases, further boosting the recruitment of key drivers of antitumor immunity with CBD-CCL4 may help to shift the balance of the tumor microenvironment to one that is more favorable to CPI therapy responsiveness.

Currently, a number of cancer immunotherapies are in preclinical and clinical development for combination with CPI therapies. However, these agents typically function by activating costimulatory receptors (e.g., Ox40, Glucocorticoid induced TNF receptor (GITR), and CD137) or blocking other inhibitory pathways (e.g., Tim3, Lag3, and Indoleamine 2,3-dioxygenase (IDO) inhibitors). Similar to blockade of PD-1/PD-L1 and CTLA4, these therapies also require the tumor to have significant immune cell infiltration. Chemokines, on the other hand, may act as a new class of immunotherapeutic agents that can be combined with many immunotherapies, as they function by specifically recruiting the key cell populations necessary for antitumor immune responses; they may also function in tumor phenotypes with poor prior immune infiltration. Thus far, using chemokines for cancer treatment has been challenging, relying on intratumoral administration or antibody-chemokine fusions for delivery to the tumor microenvironment (*42*). Our collagen-targeted delivery strategy, however, allows for systemic chemokine administration that can localize and recruit immune cells to the tumor. Thus, CBD-CCL4 may hold significant clinical potential to boost the therapeutic effect of CPI and other immunotherapies using a complementary mechanism related to other combinations currently under investigation.

In conclusion, we have demonstrated a novel method for enhancing the efficacy of CPI immunotherapy (e.g., αPD-1, αPD-L1, and αCTLA-4) through the recruitment of $CD103^+$ DCs to the tumor microenvironment using the tumor-targeted chemokine CCL4. CBD-CCL4, but not WT CCL4, significantly enhanced the immune infiltrates, including $CD103^+$ DCs and $CD8^+$ T cells, into both B16F10 and EMT6 tumors, which are cold tumor models. CBD-CCL4 markedly enhanced the antitumor effect of CPI therapy in multiple tumor models, including spontaneously developing breast cancer. This method is amenable to combination with multiple CPI antibody therapies and can be applied to multiple solid tumor types, highlighting its significant potential for clinical translation for improved cancer immunotherapies.

MATERIALS AND METHODS

Study design

This study was designed to test the efficacy of tumor-targeted delivery of CCL4 engineered to exhibit high affinity for collagen in

the tumor microenvironment. We tested whether targeted CCL4 delivery could then enhance recruitment of immune cells, including DCs and T cells, to the tumor, thus making them more responsive to CPI antibody therapy. Responses were characterized using tumor growth measurements, infiltration of immune cells into tumors, treatment-related adverse events, and cytokine production analysis. Statistical methods were not used to predetermine sample numbers; rather, pilot experiments and previously published studies were evaluated to determine appropriate numbers to yield meaningful, statistically significant results. Production of CBD-CCL4 was performed by multiple individuals, ensuring consistent and reproducible results. For animal experiments, mice were randomized into treatment groups within cages before therapy, and all mice were treated and evaluated in the same fashion. Samples were excluded from final analysis only in instances where a mouse developed health problems unrelated to the treatment, according to animal care guidelines. All tumor experiments were considered to have reached their endpoint when tumor volumes exceeded 500 mm^3. All drug administrations and histopathological analyses were done in a blinded fashion. Statistical analysis is described further in a subsequent section, and all sample numbers are depicted in the figure legends.

Production and purification of recombinant VWF A3 domain-CCL4 fusion protein

The sequence encoding for the fusion of human VWF A3 domain residues Cys^{1670}-Gly^{1874} (907 to 1111 of mature VWF), a $(GGGS)_2$ linker, and murine CCL4 was synthesized and cloned into the pcDNA3.1(+) cytomegalovirus-driven mammalian expression vector by GenScript. A sequence encoding for the 6× His-tag was added at the N terminus for downstream purification of the recombinant protein. Suspension-adapted human embryonic kidney 293F cells were maintained in serum-free FreeStyle293 Expression Medium (Gibco). Protein production was performed according to our previous protocols (*22*). Briefly, on the day of transfection, cells were transferred into fresh medium at a density of 10^6 cells/ml. Plasmid DNA (1 μg/ml) was mixed with linear 25-kDa polyethylenimine (2 μg/ml) (Polysciences) diluted in OptiPRO SFM media (Thermo Fisher Scientific), incubated for 20 min, and added dropwise to the cells [4% (v/v) final concentration]. The culture flask was agitated in a humidified orbital shaking incubator at 135 rpm at 37°C in the presence of 5% CO_2. Six days after transfection, the cell culture medium was collected, centrifuged, and filtered through a 0.22-μm filter. Culture medium was loaded into a HisTrap HP 5-ml column (GE Healthcare), using an ÄKTA pure 25 (GE Healthcare). After washing the column with wash buffer [20 mM imidazole, 20 mM NaH_2PO_4, and 0.5 M NaCl (pH 7.4)], protein was eluted with a gradient of 500 mM imidazole [in 20 mM NaH_2PO_4 and 0.5 M NaCl (pH 7.4)]. The eluted protein was further purified with size exclusion chromatography using a HiLoad Superdex 200PG column (GE Healthcare). All purification steps were carried out at 4°C. The expression of CBD-CCL4 was determined by Western blotting using anti–His-tag antibody (clone J099B12, BioLegend), and the proteins were verified as >90% pure by SDS-PAGE. Native-form murine CCL4 protein was purchased commercially from BioLegend.

SDS-PAGE analysis of protein molecular weight and purity

SDS-PAGE was performed on 4 to 20% gradient gels (Bio-Rad) after CCL4 or CBD-CCL4 was reduced with β-mercaptoethanol. After electrophoresis, gels were stained with SimplyBlue SafeStain (Thermo Fisher Scientific) according to the manufacturer's recommendations. Gel images were acquired with the ChemiDoc XRS+ system (Bio-Rad).

Dynamic light scattering of CBD-CCL4

Dynamic light scattering measurements were performed using a Zetasizer Nano ZS90 (Malvern). CBD-CCL4 (25 μg/ml CCL4 basis) was diluted in phosphate-buffered saline (PBS) or 50% mouse serum (diluted in PBS) for 30 min, after which particle size was measured in the automatic mode.

CBD-CCL4 collagen binding measurements using SPR and enzyme-linked immunosorbent assay

SPR measurements were made with a Biacore X100 SPR system (GE Healthcare). Collagen I or collagen III was immobilized via amine coupling on a CM5 chip (GE Healthcare) for ~1000 resonance units according to the manufacturer's instructions. CBD-CCL4 was flowed for 90 s (for collagen I) and for 30 s (for collagen III) at increasing concentrations in the running buffer at 30 μl/min. The sensor chip was regenerated with 50 mM NaOH for each cycle. Specific binding of CBD-CCL4 to collagen was calculated automatically using the response to a nonfunctionalized channel as a reference. Binding curves were fitted using BIAevaluation software (GE Healthcare). CBD-CCL4 binding results were fitted with Langmuir binding kinetics (1:1 binding). Enzyme-linked immunosorbent assay (ELISA) measurements were performed according to our previously reported protocol (*22*).

CBD-CCL4 binding to human and murine melanoma cryosections

Human melanoma cryosections were obtained from OriGene Technologies. Murine melanoma sections were prepared from B16F10 melanoma tumors embedded in optimal cutting temperature (OCT) compound following fixation with 10% formalin and cryopreservation in 30% sucrose. Tissue sections were blocked for 1 hour with 2% bovine serum albumin in PBS with 0.05% Tween 20 (PBS-T) at room temperature (RT), after which samples were incubated with WT CCL4 (25 μg/ml) or equimolar CBD-CCL4 in PBS-T for 2 hours at RT. Tissues were then stained with mouse anti-human CD31 (ab119339, Abcam), goat anti-mouse CCL4 (AF-451-NA, R&D Systems), and rabbit anti–collagen I antibody (ab34710, Abcam) for 1 hour at RT. After staining with the appropriate fluorescent secondary antibodies, sections were covered with ProLong Gold Antifade Mountant containing 4′,6-diamidino-2-phenylindole (DAPI) (Thermo Fisher Scientific) and sealed with a coverslip. Imaging was done with an IX83 microscope (Olympus), and images were analyzed using ImageJ software (National Institutes of Health).

GPCR calcium flux signaling assay

GPCR signaling following interaction with native-form CCL4 or CBD-CCL4 was analyzed using a calcium flux assay (FLUOFORTE Calcium Assay Kit, Enzo Life Sciences). The assay was performed according to the manufacturer's protocol with slight modifications. Reagents were reconstituted, mixed as directed, and brought to RT before use. Twenty-four hours prior, 1.5×10^5 ThP1 human monocytes, known to express CCR5 (*43*), were plated in each well of a tissue culture–treated 96-well round-bottom plate. On the day of the assay, cells were spun down at 2000 rpm for 2 min, medium

was removed, and cells were resuspended in 100 µl of assay buffer. Cells were subsequently incubated for 45 min at 37°C and then for 15 min at RT before assay. Samples were then prepared separately in PBS in triplicate and then diluted 1:4 upon addition to the cells to give the indicated molar concentration of CCL4. After the addition of the compound, the samples were mixed several times with a multichannel pipette to ensure thorough mixing, after which they were transferred to a black-walled clear-bottom 96-well plate. Calcium signaling was then measured using a Cytation 3 multimode plate reader (BioTek) at an excitation wavelength of 490 nm and an emission wavelength of 525 nm, using bottom-read optics with the gain set at 100. Median effective concentration values were calculated using a nonlinear dose-response curve fitting model comparing log (test compound) versus response in GraphPad Prism.

Tumor cell line culture and maintenance and animal sourcing

All cells were maintained in a humidified incubator at 37°C and 5% CO_2. Cells were routinely passaged using TrypLE Express (Thermo Fisher Scientific) once they reached 80 to 90% confluence. B16F10 melanoma, MMTV-PyMT breast cancer, and MC38 colon carcinoma cells were maintained in Dulbecco's modified Eagle medium (DMEM, Gibco) supplemented with 10% (v/v) fetal bovine serum (FBS; certified, U.S. origin, heat inactivated, Gibco) and (500 U/ml; 1%, v/v) penicillin-streptomycin (P/S, Gibco). EMT6 breast cancer, CT26 colon carcinoma, and ThP1 monocyte cells were maintained in RPMI 1640 (Gibco) supplemented with 10% (v/v) FBS and 1% (v/v) P/S. All cells were confirmed to be mycoplasma free using a MycoAlert PLUS mycoplasma assay (Lonza). Female C57BL/6, FVB/N, and Balb/c mice, aged 8 to 12 weeks, were obtained from the Jackson laboratory. Female FVB/N-Tg(MMTV-PyVT)634Mul/J (MMTV-PyMT) mice, aged 4 to 6 weeks, were obtained from the Jackson laboratory. MMTV-PyMT mice were inspected weekly until tumors were palpable in at least four mammary fat pads. All mice were acclimated in their cages for 72 hours before use. Treatments were randomized within cages to minimize cage-specific treatment effects. All animal experiments were performed with approval and according to the policies of the Institutional Animal Care and Use Committee at The University of Chicago.

Blood plasma half-life characterization

B16F10 melanoma cells (5×10^5) were injected intradermally on the left side of the back of each mouse. WT CCL4 and CBD-CCL4 were fluorescently labeled using Dylight 800-NHS (Thermo Fisher Scientific), and unreacted dye was removed by a Zeba Spin spin column (Thermo Fisher Scientific) according to the manufacturer's instruction. After 4 days, mice were injected with 25 µg of WT CCL4-DyLight 800 or the molar equivalent (25 µg of CCL4 basis or 93 µg of total protein) of CBD-CCL4 DyLight 800 via intravenous injection. Blood samples were collected into EDTA-containing tubes via facial bleed at 1, 5, 10, and 30 min after administration. Samples were then centrifuged at 2000 rpm for 5 min to collect plasma. Concentrations of CCL4 in plasma were measured using a LI-COR Infrared Odyssey Imager, and concentrations were calculated from a standard dilution series of labeled WT CCL4 or CBD-CCL4. Blood plasma half-life was determined using a one-phase decay model using GraphPad Prism software.

Biodistribution analysis in EMT6 tumor–bearing mice

WT CCL4 or CBD-CCL4 protein was fluorescently labeled using DyLight 647 NHS ester (Thermo Fisher Scientific), and unreacted dye was removed by a Zeba Spin spin column (Thermo Fisher Scientific) according to the manufacturer's instruction. A total of 5×10^5 EMT6 cells resuspended in 50 µl of PBS were injected subcutaneously into the mammary fat pad on the right side of each Balb/c mouse. When the tumor reached approximately 500 mm^3, 25 µg of DyLight 647–labeled CCL4 or 25 µg (6.7 µg of CCL4 basis) DyLight 647–labeled CBD-CCL4 was injected intravenously 30 min after injection, mice were euthanized, and tumors were extracted and imaged with the Xenogen IVIS Imaging System 100 (Xenogen) under the following conditions: f/stop, 2; optical filter excitation, 640 nm; emission, 670 nm; exposure time, 0.5 s; small binning. CCL4 concentration in each tumor was calculated on the basis of a standard dilution series of WT CCL4 or CBD-CCL4 labeled with DyLight 647 and normalized to the weight of the tumor.

Antitumor efficacy in B16F10 melanoma

A total of 5×10^5 B16F10 cells resuspended in 50 µl of PBS were inoculated intradermally on the left side of the back of each C57BL/6 mouse. After 4 days (or 7 days for established tumor treatment study), mice were injected with WT CCL4 (25 µg given via intravenous injection) or molar equivalent CBD-CCL4 (25 µg of CCL4 basis or 93 µg of CBD-CCL4, given via intravenous injection) in combination with CPI antibody therapy consisting of αPD-L1 and αCTLA4 (100 µg each) given via intraperitoneal injection. CPI therapy alone was administered as control. For studies performed in $Batf3^{-/-}$ mice, B16F10 cells were inoculated as above. On day 7, mice were treated as described previously. Mice were euthanized on day 11, and tumors were processed into single-cell suspensions for flow cytometry analysis. For CXCR3 blocking studies, anti-CXCR3 (clone CXCR3-173, Bio X Cell) was given at 200 µg per mouse via intraperitoneal injection, beginning on the day of treatment and continuing every 2 to 3 days for a total of three doses. Tumors were measured with a digital caliper starting 4 days after tumor inoculation, and volumes were calculated as ellipsoids, where $V = 4/3 \times \pi \times \text{depth}/2 \times \text{width}/2 \times \text{height}/2$. Mice were euthanized when tumor volume exceeded 500 mm^3 or when early removal criteria were met because of poor health of the mice. In the case of cell infiltrate analysis, mice were euthanized 10 days after tumor inoculation.

Antitumor efficacy in EMT6 breast cancer

A total of 5×10^5 EMT6 cells resuspended in 50 µl of PBS were injected subcutaneously into the mammary fat pad on the right side of each Balb/c mouse. Six and nine days after tumor inoculation, tumors were administered with WT CCL4 (25 µg given via intravenous injection) or molar equivalent CBD-CCL4 (25 µg of CCL4 basis or 93 µg of CBD-CCL4, given via intravenous injection) in combination with CPI antibody therapy consisting of αPD-L1 and αCTLA4 (100 µg each) given via intraperitoneal injection. CPI therapy alone was administered as control. Tumors were measured with a digital caliper starting 4 days after tumor inoculation as described above. Mice were euthanized 10 days after tumor inoculation to evaluate immune cell infiltration.

Immunofluorescence analysis of EMT6 breast cancer sections

After tumors were harvested, a portion of the sample was fixed in 2% paraformaldehyde (PFA) in PBS for 24 hours, after which it was immersed in 30% (v/v) sucrose for an additional 24 hours before embedding in OCT compound. Cryosections were stained as described above, with the following modifications. Primary antibody

staining cocktail consisted of rat anti-mouse CD31 (clone MEC 13.3, BD Pharmingen), rabbit anti-CD8α (ab4055, Abcam), and hamster anti-mouse CD11c (ab33483, Abcam) for 1 hour at RT. Following incubation with the appropriate secondary antibody, samples were covered with ProLong Gold Antifade Mountant with DAPI, imaged with an Olympus IX83 microscope, and processed using ImageJ software.

Analysis of treatment-related adverse events

Off-target treatment-related adverse events were analyzed in B16F10 tumor-bearing mice as previously reported (*22*). B16F10 cells (5×10^5) resuspended in 50 μl of PBS were inoculated intradermally on the left side of the back of a 15-week-old C57BL/6 mouse. Four and 7 days after inoculation, mice were injected with WT CCL4 (25 μg given via intravenous injection) or molar equivalent CBD-CCL4 (25 μg of CCL4 basis or 93 μg of CBD-CCL4, given via intravenous injection) in combination with CPI antibody therapy consisting of αPD-L1 and αCTLA4 (100 μg each) given via intraperitoneal injection. CPI therapy alone was administered as control. On day 8, blood was collected via cheek bleed into protein low-binding tubes (Eppendorf), followed by overnight incubation at 4°C. Serum cytokine concentrations were analyzed using Ready-SET-Go! ELISA kits (Invitrogen) according to the manufacturer's protocol. On day 10, mice were euthanized, and blood was again collected into protein low-binding tubes, incubated >4 hours at 4°C, and analyzed using an ALT activity assay kit (Sigma-Aldrich) according to the manufacturer's protocol. The lung, liver, and kidney were harvested and fixed overnight in 2% PFA. Samples were then embedded in paraffin blocks, 5-μm sections were cut, and sections were counterstained with hematoxylin and eosin. Samples were then imaged with a Pannoramic digital slide scanner (3DHISTECH), and images were evaluated by a pathologist (A.I.) blinded to the treatment groups.

Antitumor efficacy in CT26 and MC38 colon carcinoma

A total of 5×10^5 CT26 or MC38 cells resuspended in 50 μl of PBS were inoculated intradermally on the left side of the back of each Balb/c (for CT26) or C57BL/6 (for MC38) mouse. After 5 days, mice were injected with unmodified CCL4 (25 μg given via intravenous injection) or molar equivalent CBD-CCL4 (25 μg of CCL4 basis or 93 μg of CBD-CCL4, given via intravenous injection) in combination with 100 μg of αPD-1 antibody therapy given via intraperitoneal injection. Tumors were measured with a digital caliper starting 5 days after tumor inoculation as described above. Mice were euthanized when tumor volume exceeded 500 mm^3.

Antitumor efficacy in MMTV-PyMT breast cancer

For orthotopic implantable MMTV-PyMT studies, a total of 10^6 MMTV-PyMT cells resuspended in 50 μl of PBS were inoculated subcutaneously into the mammary fat pad on the right side of each FVB/N mouse. After 6 days, mice were injected with unmodified CCL4 (25 μg given via intravenous injection) or molar equivalent CBD-CCL4 (25 μg of CCL4 basis or 93 μg of CBD-CCL4, given via intraveous injection) in combination with CPI antibody therapy consisting of αPD-L1 and αCTLA4 (100 μg each) given via intraperitoneal injection. Tumors were measured with a digital caliper starting 5 days after tumor inoculation as described above. Mice were euthanized when tumor volume exceeded 500 mm^3. For tumor rechallenge experiments, mice that cleared tumors were inoculated 1 month after tumors were last palpable in the contralateral mammary fat pad with a total of 10^6 MMTV-PyMT cells resuspended in 50 μl of PBS. Naïve control mice were also inoculated in a similar fashion. The mice were evaluated every 3 days beginning 5 days after tumor inoculation for the development of tumors. For spontaneous MMTV-PyMT tumor studies, once total tumor volume reached approximately 100 mm^3, the mice were treated with CBD-CCL4 (25 μg of CCL4 basis or 93 μg of CBD-CCL4, given via intravenous injection) in combination with CPI antibody therapy consisting of αPD-L1 and αCTLA4 (100 μg each) given via intraperitoneal injection. Identical treatments were given 7 and 14 days after initial therapy. Tumors were measured biweekly with a digital caliper as described above, and the mice were euthanized once tumor volume exceeded 1000 mm^3 or the mice experienced adverse effects due to tumor burden.

Tissue and single-cell preparation for immune cell analysis

Both B16F10 and EMT6 tumors were harvested 10 days after initial tumor inoculation. All cell isolation procedures were adapted from previously reported methods (*22*). Tumors were minced into small pieces, after which enzymatic digestion consisting of collagenase D (2 mg/ml) and deoxyribonuclease I (40 μg/ml, Roche) in DMEM containing 2% FBS was performed for 30 min at 37°C under gentle agitation. Single-cell suspensions were obtained by gently disrupting the enzyme-treated tumor through a 70-μm cell strainer. Red blood cells were lysed with ammonium-chloride-potassium (ACK) lysing buffer (Quality Biological), after which cells were centrifuged and resuspended in flow cytometry staining buffer consisting of PBS containing 2% FBS for downstream analysis.

MMTV-PyMT splenocyte stimulation assay

Spleens were harvested 21 days following secondary challenge of MMTV-PyMT tumor cells. Single-cell suspensions of splenocytes were obtained by passing each spleen over a 70-μm cell strainer, after which red blood cells were lysed with ACK lysing buffer. Cells were centrifuged, passed over a 70-μm cell strainer again, and resuspended at 1×10^7 cells/ml in Iscove's modified Dulbecco's medium (Gibco). Splenocytes (10^6) were then plated in 96-well round-bottom plates in the presence of PMA (20 ng/ml) and ionomycin (1 μg/ml) for 6 hours at 37°C. BD Golgiplug (BD Biosciences) protein transport inhibitor was added during the last 4 hours of culture. Cells were then centrifuged and resuspended in flow cytometry staining buffer for downstream analysis. Intracellular cytokine staining was performed using the BD Cytofix/Cytoperm (BD Biosciences) intracellular staining kit according to the manufacturer's protocol.

Flow cytometry analysis and antibodies used

Single-cell suspensions from tumors were prepared as described above. Antibodies against the following molecules were used in all experiments: anti-mouse CD3 (145-2C11, BD Biosciences), anti-mouse CD4 (RM4-5, BD Biosciences), anti-mouse CD8 (53-6.7, BD Biosciences), anti-mouse CD25 (PC61, BD Biosciences), anti-mouse CD45 (30-F11, BioLegend), anti-mouse CD44 (IM7, BioLegend), anti-mouse CD62L (MEL-14, BD Biosciences), anti-mouse PD-1 (29F.1A12, BioLegend), anti-mouse NK1.1 (PK136, BioLegend), anti-mouse FoxP3 (MF23, BD Biosciences), anti-mouse TNFα (MP6-XT22, eBioscience), anti-mouse IFN-γ (XMG1.2, BioLegend), anti-mouse F4/80 (BM8, BioLegend), anti-mouse MHCII (M5/114.15.2, BioLegend), anti-mouse CD11b (M1/70, BioLegend), anti-mouse CD11c (N418, BioLegend), anti-mouse CD19 (1D3, BD Biosciences),

anti-mouse Gr-1 (RB6-8C5, BioLegend), anti-mouse CCR5 (HM-CCR5, BioLegend), and anti-mouse CD103 (M290, BD Biosciences). Live/dead cell discrimination was performed using Fixable Viability Dye eFluor 455 (eBioscience) according to the manufacturer's instructions; an F_c receptor blocking step (anti-mouse CD16/32, clone 93, BioLegend) was also included to minimize nonspecific antibody binding. Surface staining was carried out on ice for 20 min, and intracellular staining was performed using the FoxP3-transcription factor staining kit according to the manufacturer's instructions (eBioscience). Otherwise, samples were fixed in 2% PFA in PBS. All flow cytometric analyses were done using a Fortessa (BD Biosciences) flow cytometer and analyzed using FlowJo software (TreeStar).

Statistical analysis

The statistical significance between treatment groups was assessed using Prism software (v7, GraphPad). For multiple comparisons, analysis of variance (ANOVA) followed by Tukey's post hoc test was used when differences between groups were found to be similar by Brown-Forsythe test. For nonparametric data, Kruskal-Wallis test followed by Dunn's multiple comparisons test was used. For comparisons between two groups, a two-tailed Student's *t* test was used. Survival curves were analyzed using the log-rank (Mantel-Cox) test. $*P < 0.05$ and $**P < 0.01$.

SUPPLEMENTARY MATERIALS

Supplementary material for this article is available at http://advances.sciencemag.org/cgi/content/full/5/12/eaay1357/DC1

Fig. S1. Dynamic light scattering measurement of CBD-CCL4.
Fig. S2. Binding of CBD-CCL4 and WT CCL4 to collagen and murine melanoma sections.
Fig. S3. In vivo imaging of EMT6 tumors.
Fig. S4. Representative flow cytometry gating strategy.
Fig. S5. Cell infiltrate analysis of effector T cells, MDSCs, and macrophages in B16F10 melanoma.
Fig. S6. Immunofluorescence analysis of $CD8^+$ cells and $CD11c^+$ DCs in EMT6 breast cancer.
Fig. S7. Tumor growth curves of CT26 and MC38 following treatment with anti–PD-1 + CBD-CCL4.
Fig. S8. CCR5 expression on T cells and DCs.
Fig. S9. Survival curves of spontaneous MMTV-PyMT mice following treatment.
Table S1. Sequences of CCL4, CBD protein, and CBD-CCL4 fusion protein.

View/request a protocol for this paper from *Bio-protocol*.

REFERENCES AND NOTES

1. S. Farkona, E. P. Diamandis, I. M. Blasutig, Cancer immunotherapy: The beginning of the end of cancer? *BMC Med.* **14**, 73 (2016).
2. A. Ribas, J. D. Wolchok, Cancer immunotherapy using checkpoint blockade. *Science* **359**, 1350–1355 (2018).
3. R. W. Jenkins, D. A. Barbie, K. T. Flaherty, Mechanisms of resistance to immune checkpoint inhibitors. *Br. J. Cancer* **118**, 9–16 (2018).
4. J. Larkin, V. Chiarion-Sileni, R. Gonzalez, J. J. Grob, C. L. Cowey, C. D. Lao, D. Schadendorf, R. Dummer, M. Smylie, P. Rutkowski, P. F. Ferrucci, A. Hill, J. Wagstaff, M. S. Carlino, J. B. Haanen, M. Maio, I. Marquez-Rodas, G. A. McArthur, P. A. Ascierto, G. V. Long, M. K. Callahan, M. A. Postow, K. Grossmann, M. Sznol, B. Dreno, L. Bastholt, A. Yang, L. M. Rollin, C. Horak, F. S. Hodi, J. D. Wolchok, Combined nivolumab and ipilimumab or monotherapy in untreated melanoma. *N. Engl. J. Med.* **373**, 23–34 (2015).
5. M. J. Smyth, S. F. Ngiow, A. Ribas, M. W. Teng, Combination cancer immunotherapies tailored to the tumour microenvironment. *Nat. Rev. Clin. Oncol.* **13**, 143–158 (2016).
6. P. L. Chen, W. Roh, A. Reuben, Z. A. Cooper, C. N. Spencer, P. A. Prieto, J. P. Miller, R. L. Bassett, V. Gopalakrishnan, K. Wani, M. P. De Macedo, J. L. Austin-Breneman, H. Jiang, Q. Chang, S. M. Reddy, W. S. Chen, M. T. Tetzlaff, R. J. Broaddus, M. A. Davies, J. E. Gershenwald, L. Haydu, A. J. Lazar, S. P. Patel, P. Hwu, W. J. Hwu, A. Diab, I. C. Glitza, S. E. Woodman, L. M. Vence, I. I. Wistuba, R. N. Amaria, L. N. Kwong, V. Prieto, R. E. Davis, W. Ma, W. W. Overwijk, A. H. Sharpe, J. Hu, P. A. Futreal, J. Blando, P. Sharma, J. P. Allison, L. Chin, J. A. Wargo, Analysis of immune signatures in longitudinal tumor samples yields insight into biomarkers of response and mechanisms of resistance to immune checkpoint blockade. *Cancer Discov.* **6**, 827–837 (2016).
7. J. Li, K. T. Byrne, F. Yan, T. Yamazoe, Z. Chen, T. Baslan, L. P. Richman, J. H. Lin, Y. H. Sun, A. J. Rech, D. Balli, C. A. Hay, Y. Sela, A. J. Merrell, S. M. Liudahl, N. Gordon, R. J. Norgard, S. Yuan, S. Yu, T. Chao, S. Ye, T. S. K. Eisinger-Mathason, R. B. Faryabi, J. W. Tobias, S. W. Lowe, L. M. Coussens, E. J. Wherry, R. H. Vonderheide, B. Z. Stanger, Tumor cell-intrinsic factors underlie heterogeneity of immune cell infiltration and response to immunotherapy. *Immunity* **49**, 178–193.e7 (2018).
8. M. Binnewies, E. W. Roberts, K. Kersten, V. Chan, D. F. Fearon, M. Merad, L. M. Coussens, D. I. Gabrilovich, S. Ostrand-Rosenberg, C. C. Hedrick, R. H. Vonderheide, M. J. Pittet, R. K. Jain, W. Zou, T. K. Howcroft, E. C. Woodhouse, R. A. Weinberg, M. F. Krummel, Understanding the tumor immune microenvironment (TIME) for effective therapy. *Nat. Med.* **24**, 541–550 (2018).
9. J. A. Trujillo, R. F. Sweis, R. Bao, J. J. Luke, T cell-inflamed versus non-T cell-inflamed tumors: A conceptual framework for cancer immunotherapy drug development and combination therapy selection. *Cancer Immunol. Res.* **6**, 990–1000 (2018).
10. R. R. Ji, S. D. Chasalow, L. Wang, O. Hamid, H. Schmidt, J. Cogswell, S. Alaparthy, D. Berman, M. Jure-Kunkel, N. O. Siemers, J. R. Jackson, V. Shahabi, An immune-active tumor microenvironment favors clinical response to ipilimumab. *Cancer Immunol. Immunother.* **61**, 1019–1031 (2012).
11. N. Nagarsheth, M. S. Wicha, W. Zou, Chemokines in the cancer microenvironment and their relevance in cancer immunotherapy. *Nat. Rev. Immunol.* **17**, 559–572 (2017).
12. D. S. Chen, I. Mellman, Elements of cancer immunity and the cancer-immune set point. *Nature* **541**, 321–330 (2017).
13. S. Spranger, T. F. Gajewski, Tumor-intrinsic oncogene pathways mediating immune avoidance. *Oncoimmunology* **5**, e1086862 (2016).
14. H. Tang, Y. Wang, L. K. Chlewicki, Y. Zhang, J. Guo, W. Liang, J. Wang, X. Wang, Y. X. Fu, Facilitating T cell infiltration in tumor microenvironment overcomes resistance to PD-L1 blockade. *Cancer Cell* **29**, 285–296 (2016).
15. J. P. Bottcher, E. S. C. Reis, The role of type 1 conventional dendritic cells in cancer immunity. *Trends Cancer* **4**, 784–792 (2018).
16. E. W. Roberts, M. L. Broz, M. Binnewies, M. B. Headley, A. E. Nelson, D. M. Wolf, T. Kaisho, D. Bogunovic, N. Bhardwaj, M. F. Krummel, Critical role for $CD103^+/CD141^+$ dendritic cells bearing CCR7 for tumor antigen trafficking and priming of T cell immunity in melanoma. *Cancer Cell* **30**, 324–336 (2016).
17. H. Salmon, J. Idoyaga, A. Rahman, M. Leboeuf, R. Remark, S. Jordan, M. Casanova-Acebes, M. Khudoynazarova, J. Agudo, N. Tung, S. Chakarov, C. Rivera, B. Hogstad, M. Bosenberg, D. Hashimoto, S. Gnjatic, N. Bhardwaj, A. K. Palucka, B. D. Brown, J. Brody, F. Ginhoux, M. Merad, Expansion and activation of $CD103^+$ dendritic cell progenitors at the tumor site enhances tumor responses to therapeutic PD-L1 and BRAF inhibition. *Immunity* **44**, 924–938 (2016).
18. M. Merad, P. Sathe, J. Helft, J. Miller, A. Mortha, The dendritic cell lineage: Ontogeny and function of dendritic cells and their subsets in the steady state and the inflamed setting. *Annu. Rev. Immunol.* **31**, 563–604 (2013).
19. S. Spranger, D. Dai, B. Horton, T. F. Gajewski, Tumor-residing Batf3 dendritic cells are required for effector T cell trafficking and adoptive T cell therapy. *Cancer Cell* **31**, 711–723.e4 (2017).
20. S. Spranger, R. Bao, T. F. Gajewski, Melanoma-intrinsic β-catenin signalling prevents anti-tumour immunity. *Nature* **523**, 231–235 (2015).
21. R. S. Riley, C. H. June, R. Langer, M. J. Mitchell, Delivery technologies for cancer immunotherapy. *Nat. Rev. Drug Discov.* **18**, 175–196 (2019).
22. J. Ishihara, A. Ishihara, K. Sasaki, S.-Y. Lee, J.-M. Williford, M. Yasui, H. Abe, L. Potin, P. Hosseinchi, K. Fukunaga, M. M. Raczy, L. T. Gray, A. Mansurov, K. Katsumata, M. Fukayama, S. J. Kron, M. A. Swartz, J. A. Hubbell, Targeted antibody and cytokine cancer immunotherapies through collagen affinity. *Sci. Transl. Med.* **11**, eaau3259 (2019).
23. J. A. Nagy, S. H. Chang, A. M. Dvorak, H. F. Dvorak, Why are tumour blood vessels abnormal and why is it important to know? *Br. J. Cancer* **100**, 865–869 (2009).
24. H. Liang, X. Li, B. Wang, B. Chen, Y. Zhao, J. Sun, Y. Zhuang, J. Shi, H. Shen, Z. Zhang, J. Dai, A collagen-binding EGFR antibody fragment targeting tumors with a collagen-rich extracellular matrix. *Sci. Rep.* **6**, 18205 (2016).
25. N. Momin, N. K. Mehta, N. R. Bennett, L. Ma, J. R. Palmeri, M. M. Chinn, E. A. Lutz, B. Kang, D. J. Irvine, S. Spranger, K. D. Wittrup, Anchoring of intratumorally administered cytokines to collagen safely potentiates systemic cancer immunotherapy. *Sci. Transl. Med.* **11**, eaaw2614 (2019).
26. A. S. Ribba, I. Loisel, J. M. Lavergne, I. Juhan-Vague, B. Obert, G. Cherel, D. Meyer, J. P. Girma, Ser968Thr mutation within the A3 domain of von Willebrand factor (VWF) in two related patients leads to a defective binding of VWF to collagen. *Thromb. Haemost.* **86**, 848–854 (2001).
27. G. Alkhatib, The biology of CCR5 and CXCR4. *Curr. Opin. HIV AIDS* **4**, 96–103 (2009).
28. Y. K. Chae, A. Arya, W. Iams, M. R. Cruz, S. Chandra, J. Choi, F. Giles, Current landscape and future of dual anti-CTLA4 and PD-1/PD-L1 blockade immunotherapy in cancer; lessons learned from clinical trials with melanoma and non-small cell lung cancer (NSCLC). *J. Immunother. Cancer* **6**, 39 (2018).

29. J. Gong, A. Chehrazi-Raffle, S. Reddi, R. Salgia, Development of PD-1 and PD-L1 inhibitors as a form of cancer immunotherapy: A comprehensive review of registration trials and future considerations. *J. Immunother. Cancer* **6**, 8 (2018).
30. M. G. Lechner, S. S. Karimi, K. Barry-Holson, T. E. Angell, K. A. Murphy, C. H. Church, J. R. Ohlfest, P. Hu, A. L. Epstein, Immunogenicity of murine solid tumor models as a defining feature of in vivo behavior and response to immunotherapy. *J. Immunother.* **36**, 477–489 (2013).
31. J. Ishihara, K. Fukunaga, A. Ishihara, H. M. Larsson, L. Potin, P. Hosseinchi, G. Galliverti, M. A. Swartz, J. A. Hubbell, Matrix-binding checkpoint immunotherapies enhance antitumor efficacy and reduce adverse events. *Sci. Transl. Med.* **9**, (2017).
32. B. Wang, Q. Li, L. Qin, S. Zhao, J. Wang, X. Chen, Transition of tumor-associated macrophages from MHC class II^{hi} to MHC class II^{low} mediates tumor progression in mice. *BMC Immunol.* **12**, 43 (2011).
33. S. Mariathasan, S. J. Turley, D. Nickles, A. Castiglioni, K. Yuen, Y. Wang, E. E. Kadel III, H. Koeppen, J. L. Astarita, R. Cubas, S. Jhunjhunwala, R. Banchereau, Y. Yang, Y. Guan, C. Chalouni, J. Ziai, Y. Senbabaoglu, S. Santoro, D. Sheinson, J. Hung, J. M. Giltnane, A. A. Pierce, K. Mesh, S. Lianoglou, J. Riegler, R. A. D. Carano, P. Eriksson, M. Hoglund, L. Somarriba, D. L. Halligan, M. S. van der Heijden, Y. Loriot, J. E. Rosenberg, L. Fong, I. Mellman, D. S. Chen, M. Green, C. Derleth, G. D. Fine, P. S. Hegde, R. Bourgon, T. Powles, TGFβ attenuates tumour response to PD-L1 blockade by contributing to exclusion of T cells. *Nature* **554**, 544–548 (2018).
34. K. Hildner, B. T. Edelson, W. E. Purtha, M. Diamond, H. Matsushita, M. Kohyama, B. Calderon, B. U. Schraml, E. R. Unanue, M. S. Diamond, R. D. Schreiber, T. L. Murphy, K. M. Murphy, Batf3 deficiency reveals a critical role for CD8α^{+} dendritic cells in cytotoxic T cell immunity. *Science* **322**, 1097–1100 (2008).
35. B. Lee, M. Sharron, L. J. Montaner, D. Weissman, R. W. Doms, Quantification of CD4, CCR5, and CXCR4 levels on lymphocyte subsets, dendritic cells, and differentially conditioned monocyte-derived macrophages. *Proc. Natl. Acad. Sci. U.S.A.* **96**, 5215–5220 (1999).
36. Y. Nakamura, A. Mochida, P. L. Choyke, H. Kobayashi, Nanodrug delivery: Is the enhanced permeability and retention effect sufficient for curing cancer? *Bioconjug. Chem.* **27**, 2225–2238 (2016).
37. S. K. Golombek, J. N. May, B. Theek, L. Appold, N. Drude, F. Kiessling, T. Lammers, Tumor targeting via EPR: Strategies to enhance patient responses. *Adv. Drug Deliv. Rev.* **130**, 17–38 (2018).
38. A. Fantozzi, G. Christofori, Mouse models of breast cancer metastasis. *Breast Cancer Res.* **8**, 212 (2006).
39. E. Y. Lin, J. G. Jones, P. Li, L. Zhu, K. D. Whitney, W. J. Muller, J. W. Pollard, Progression to malignancy in the polyoma middle T oncoprotein mouse breast cancer model provides a reliable model for human diseases. *Am. J. Pathol.* **163**, 2113–2126 (2003).
40. D. S. Pisal, M. P. Kosloski, S. V. Balu-Iyer, Delivery of therapeutic proteins. *J. Pharm. Sci.* **99**, 2557–2575 (2010).
41. E. Ruoslahti, S. N. Bhatia, M. J. Sailor, Targeting of drugs and nanoparticles to tumors. *J. Cell Biol.* **188**, 759–768 (2010).
42. C. Hess, D. Neri, Evaluation of antibody-chemokine fusion proteins for tumor-targeting applications. *Exp. Biol. Med.* **239**, 842–852 (2014).
43. M. Gouwy, S. Struyf, N. Berghmans, C. Vanormelingen, D. Schols, J. Van Damme, CXCR4 and CCR5 ligands cooperate in monocyte and lymphocyte migration and in inhibition of dual-tropic (R5/X4) HIV-1 infection. *Eur. J. Immunol.* **41**, 963–973 (2011).

Acknowledgments: We would like to thank the Human Tissue Resource Center of the University of Chicago for histology analysis, A. Solanki for tail vein injections, and S. Gomes, S. MacEwan, E. Watkins, and K. Sasaki for experimental assistance and helpful discussion. **Funding:** This work was supported by funds from the University of Chicago.
Author contributions: J.-M.W., J.I., M.A.S., and J.A.H. designed the project. J.-M.W. and J.I. performed the experiments. J.-M.W., J.I., A.I., and J.A.H. analyzed the data. J.-M.W., J.I., and J.A.H. wrote the paper. A.M., P.H., T.M.M., and L.P. assisted with tumor experiments and protein production. A.I. performed the histopathological analysis. **Competing interests:** J.I., A.I., M.A.S., and J.A.H. are inventors on U.S. Provisional Patent applications 62/638,520, 28/984,351, and 62/727,156. J.I., A.I., M.A.S., and J.A.H. are founders and shareholders in Arrow Immune Inc., which is developing the technology presented in this report. The other authors declare that they have no competing interests. **Data and materials availability:** All data needed to evaluate the conclusions in the paper are present in the paper and/or the Supplementary Materials. Additional data related to this paper may be requested from the authors.

Submitted 31 May 2019
Accepted 21 October 2019
Published 11 December 2019
10.1126/sciadv.aay1357

Citation: J.-M. Williford, J. Ishihara, A. Ishihara, A. Mansurov, P. Hosseinchi, T. M. Marchell, L. Potin, M. A. Swartz, J. A. Hubbell, Recruitment of CD103^{+} dendritic cells via tumor-targeted chemokine delivery enhances efficacy of checkpoint inhibitor immunotherapy. *Sci. Adv.* **5**, eaay1357 (2019).